KAWASAKI STEEL TECHNICAL REPORT
No.40 (May 1999)
Steinless Steel and Steel Platel

Microstructure Control for Improving Sour Resistance of Pressure Vessel Steel Plates and Their Performance

Fumimaru Kawabata, Osamu Tanigawa, Ichiro Nakagawa

Synopsis :
This paper examined technologies to advance the pressure vessel steels in the resistance to hydrogen-induced cracking (HIC) and sulfide stress corrosion cracking (SSC) and to make them applicable in wet H2S environments. The heavy gauge plates of ASTM A516-70 grade up to 127 mm in thickness and the A841 cl.l grade of 50.8 mm in thickness with high welding performance have been manufactured with such technologies. HIC resistance has been remarkably improved by reducing the sulfur content and the clustering-free shape-control of MnS, the latter of which is carried out with the ACR value control (1 to 3) by the addition of Ca. The effectiveness of the thermo-mechanical control process (TMCP) in preventing SOHIC was indicated by the model and was proved for the new A841 steel plate of the TMCP type.

The body can be viewed from the next page.

Microstructure Control for Improving Sour Resistance of Pressure Vessel Steel Plates and Their Performance*

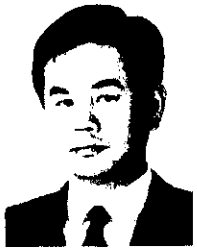
Fumimaru Kawabata
Dr. Eng.,
Senior Researcher,
Plate & Shape Lab.,
Technical Res. Labs.


Osamu Tanigawa
Staff Assistante General Manager, Plate, Casting & Forging Control Sec., Technical Control Dept.,
Mizushima Works


Ichiro Nakagawa
Staff Manager,
Technical Service Sec.,
Technical Control Dept.,
Mizushima Works

Synopsis:

This paper examined technologies to advance the pressure vessel steels in the resistance to hydrogen-induced cracking (HIC) and sulfide stress corrosion cracking (SSC) and to make them applicable in wet H_2S environments. The heavy gauge plates of ASTM A516–70 grade up to 127 mm in thickness and the A841 cl.1 grade of 50.8 mm in thickness with high welding performance have been manufactured with such technologies. HIC resistance has been remarkably improved by reducing the sulfur content and the clustering-free shape-control of MnS, the latter of which is carried out with the ACR value control (1 to 3) by the addition of Ca. The effectiveness of the thermo-mechanical control process (TMCP) in preventing SOHIC was indicated by the model and was proved for the new A841 steel plate of the TMCP type.

1 Introduction

The steels that have been used in the current pressure vessels for approximately 20 years are so old that they might have lost their resistance to stringent wet H_2S environments; in fact, some of them have reportedly been damaged by hydrogen-induced cracking (HIC) and are in serious condition. In addition to these issues, the current pressure vessel engineering needs higher strength and heavier thickness for the plates, such as ASTM A516–70 or A841 grade, as well as strong resistance to HIC.

This paper first examines the mechanisms of SOHIC (stress oriented HIC), which is most dangerous and fatal to vessels, with some emphasis on the analytical factors of the microstructure that are based on the studies of linepipe steel plates as they concern such essential factors as cleanliness and inclusion shape control. The developed ASTM A516–70 and A841 grades steels, of 127 and 50.8 mm in respective maximum thickness, are shown to have superior properties.

2 Enhancement of HIC and SOHIC Resistance —Types of Cracking in Wet H_2S Environments—

Two types of cracking have been observed for steels exposed to wet H_2S environments. One type is called HIC, which takes place regardless of stress. HIC in this category includes both the blisters near the surface of the plate and planar cracks. HIC changes its cracking behavior with stress into something usually called SOHIC, which propagates stepwise. The other is SSC, which originates under stress in some cases together with hydrogen embrittlement. The latter type of cracking is likely to occur in high strength steels, such as those for OCTG.

The typical cracking behaviors of these cracks are illustrated in **Fig. 1**. HIC of SOHIC type consists of the small HIC units aligning perpendicular to the applied stress. It is usually SOHIC type that occurs in relatively low strength steels[1,2] such as those for pressure vessels or linepipes.

3 Improvement of HIC Resistance

The elemental concentration distributions were mea-

* Originally published in *Kawasaki Steel Giho*, **30**(1998)3, 154–161

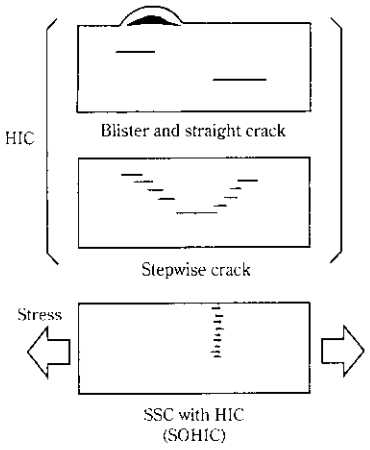

Fig. 1 Typical examples of hydrogen-induced cracking encountered for HSLA steels

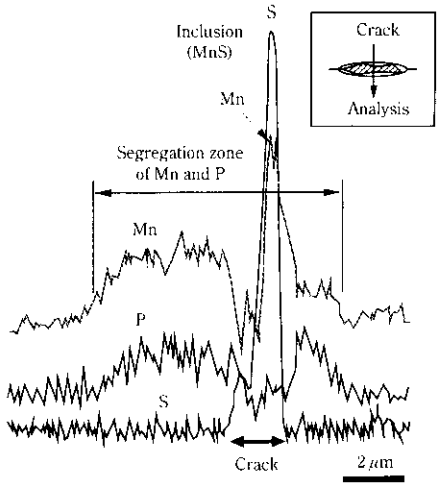

Fig. 2 Segregation of specific elements inside and in the vicinity of an HIC

sured by electron probe micro-analysis across an HIC and are shown in **Fig. 2**. Here observed are positive segregations of Mn and P around HIC. In this case, the existence of MnS inclusion in HIC was verified by the high peaks of Mn and S and regarded as the initiation site of HIC[3,4]. The MnS inclusion reportedly has a strong trigger effect on the crack initiation due to its sharpness caused by elongation in rolling.

The size minimization of MnS resulting from reduction of the S content is quite effective in reducing HIC susceptibility. **Figure 3** demonstrates the dramatic decrease in the crack area ratio (defined later) with the reduction of the S content down to 10 ppm. However, it levels off below 10 ppm. In this low S content range, prevention against sharpening, *i.e.* spheroidizing of the inclusion, is also effective in reducing HIC susceptibility. This shape control of MnS is carried out by adding Ca, called 'Ca-treatment'. Calcium has higher affinity to both O and S than Mn. CaO, which is spherical, forms first at higher temperature, then CaS is formed on the spherical surface of CaO, which is less ductile at rolling temperature.

However, the massive addition of Ca to deal with a large amount of S in steel creates many clusters of CaO. These clusters also initiate HIC in the same manner as the elongated MnS inclusions. The shape control mentioned here is now being perfectly carried out by controlling the atomic concentration ratio (ACR) which is defined by Eq. (1) in the optimum range[5-7].

$$ACR = \frac{\%Ca - (0.18 + 130 \cdot \%Ca) \cdot \%O}{1.25 \cdot \%S} \quad \cdots (1)$$

Here, Ca_{eff} is the effective amount available for CaO to form CaS after consumption. Ca-Si powder is injected into the molten steel in the final stage of the steelmaking. In the injecting process, the S content, which most affects the ACR value, is analyzed continually through injection to determine the optimum amount of Ca to inject.

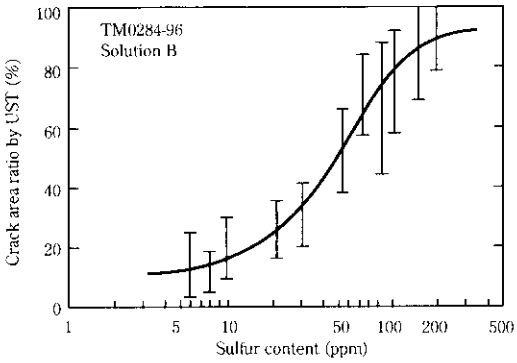

Fig. 3 Enhancement of HIC-resistance of steel by reducing sulfur content

The relationship between the ACR value and HIC resistance is cleatly observed in the production of the API 5L-X46 and X60 linepipe steels for sour services, as shown in **Fig. 4**. HIC tests were carried out by the procedure of NACE TM0284–96 with solution B. HIC resistance was evaluated by the crack area detected by an ultrasonic scanning test (UST). The crack area ratio (CAR) is defined as the ratio of the total projected crack area to the surface area of a test coupon as shown in **Fig. 5**. Figure 4 indicates that the CAR was minimized when the ACR values lay in the optimum range from 1 to 3. The CAR value increased outside of the optimum ACR range. For too small ACR values, the amount of Ca was in short for complete shape control, while excessive Ca formed oxide clusters when ACR values were too large.

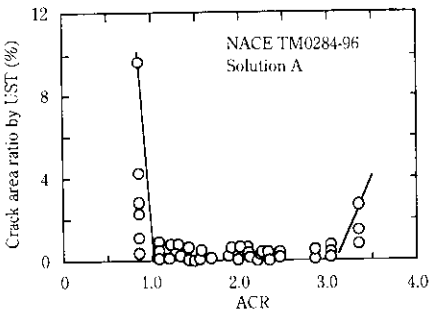

Fig. 4 Optimum range of ACR value for enhancement of HIC-resistance of steel of API5L-X46–60 grades

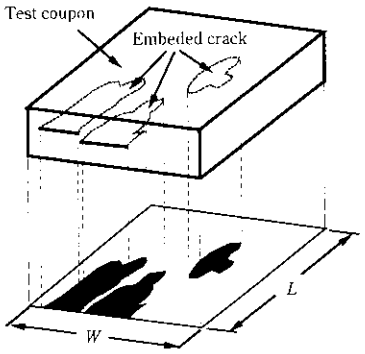

$$CAR = \frac{\text{Total projected crack area, } \Sigma S_i}{\text{Area of specimen, } L \times W} \times 100\ (\%)$$

Fig. 5 Measurement of crack area ratio (CAR) of embeded HICs by scanning ultra-sonic test (UST)

4 Enhancement of SOHIC Resistance

4.1 Cracking Behavior of SOHIC

SOHIC is caused by stress. It shows behavior such as that illustrated in **Photo 1**, which shows the typical one observed by the method A in NACE TM0177–96[8] with solution A. SOHIC units and HICs are much alike in appearance but SOHIC units stack in the thickness direction. For HICs with no stress, no such behavior has been reported. This characteristic cracking behavior suggests that the stress induces SOHIC because it raises the mobility of atomic hydrogen on the slip plane with the help of the mobile dislocations and induces the accumulation to the initiation sites.

4.2 Latent Initiation Site Model for SOHIC Mechanism

The specific orientation to the stress direction in the crack alignment of SOHIC suggests some particular sites are latent but may be activated by the stress. Calculations indicated that high hydrogen vapor pressure in an HIC makes the surrounding area yielded, in which the

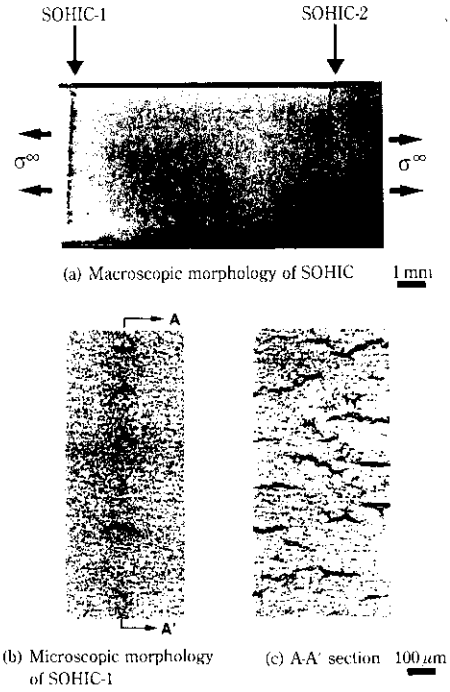

Photo 1 Typical SOHIC behavior observed for an API 5LX46 line pipe steel tested by TM0177–96 Method A with the solution A

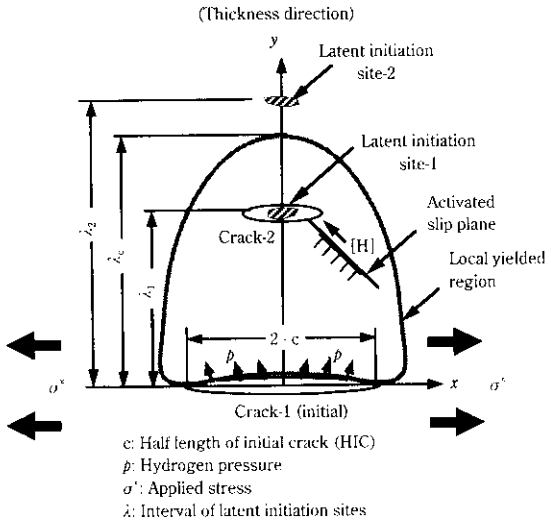

Fig. 6 Schematic explanation of the "latent initiation site model"

interaction between the dislocations and the atomic hydrogen is activated. These calculations have given us one understanding of the peculiar behavior of SOHIC, that is the "latent initiation site model"[9], which is illustrated in **Fig. 6**. The model assumes that an initial $2 \cdot c$ long 'Crack-1' already exists. The interaction between the hydrogen pressure 'p' in Crack-1 and the applied stress 'σ^{∞}' creates an yielded region around Crack-1,

which is circumscribed by a broken contour. When a latent initiation 'Site-1' lies in the yielded region, that is, in the position where $\lambda_1 > \lambda_c$, it begins to accumulate atomic hydrogen and eventually causes 'Crack-2' because the mobility of the free hydrogen atoms '[H]' is raised with the help of the mobile dislocations on the slip plane activated by yielding. Thus, this type of crack is called "stress-assisted HIC". Another 'Site-2' is latent and will not cause a crack as long as it lies outside of the yielded region if $\lambda_2 > \lambda_c$. When Crack-2 occurs and another yielded region emerges to include Site-2, Site-2 may cause a crack. A chain-like process will occur for propagation. The particles of CaO, CaS, and Al_2O_3 usually work as the laten initiation sites, and some stress-assisted HICs have been observed at pearlite colonies as well.

4.3 Preventive Condition to SOHIC Attack

The maximum shear stress, τ_{max}, around a crack is calculated in the plane strain condition[5] where a crack lies on the x-axis and its center is placed at the origin of the x-y coordinates. The value of τ_{max}, is given by Eq. (2)[10]. The value of p is the hydrogen pressure inside the crack and σ^∞ is the applied stress in the x-direction.

$$\tau_{max} = \sqrt{{\tau_{xy}}^2 + \left(\frac{\sigma_y - \sigma_x}{2}\right)^2} \cdots\cdots\cdots\cdots (2)$$

where

$$\sigma_y - \sigma_x + 2i\tau_{xy} = -\sigma^\infty - 2iy\frac{dw(z)}{dz},\ i = \sqrt{-1} \cdots (3)$$

$$w(z) = p\left(\frac{z}{\sqrt{z^2 - c^2}} - 1\right),\ z = x + iy \cdots\cdots\cdots (4)$$

The yielded region around the initial crack is depictable using Tresca's yielding condition where σ_s exceeds $2 \cdot \tau_{max}$. The yielding area is shown in **Fig. 7** as the shaded region on the assumption that $\sigma_s = 490$ MPa and $p = 980$ MPa[11]. The dimensions are normalized by the initial crack length $2 \cdot c$. In this case, $\sigma^\infty = 0$ corresponds to HIC test and $\sigma^\infty = 245$ MPa to the SSC test. The apparent difference between these cases is in the extension of the yielded region in the thickness direction (the y-direction, here). The extension of the yielded region, λ_c, is an index for the start of the above-mentioned chain-like propagation and is given by Eq. (5), which is a function of the half crack length (c), the yield stress of the meterial (σ_s), the applied stress (σ^∞), and the hydrogen pressure (p).

$$\frac{\sigma_s}{2} = \frac{p\lambda_c^*}{(1 + \lambda_c^{*2})^{\frac{1}{2}}} + \frac{\sigma^\infty}{2},\ \lambda_c^* \equiv \frac{\lambda_c}{c} \cdots\cdots\cdots\cdots (5)$$

The threshold stress (σ_f), which is the minimum stress to failure of SOHIC and is obtained by the SSC test of the tensile type in accordance with NACE TM0177–96

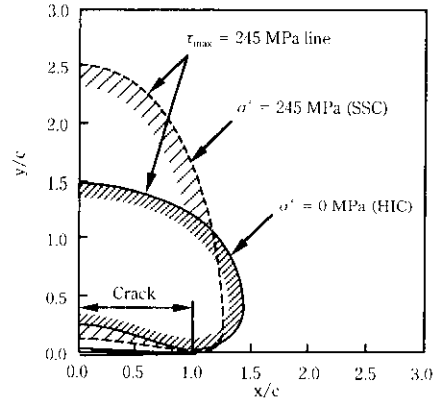

Fig. 7 Calculation example of yielded region profiles in cases of being in no stress ($\sigma^\infty = 0$) and applied stress ($\sigma^\infty = 245$ MPa)

Method A, can be related to the material by the latent initiation site model. Assuming that the initiation condition of SOHIC results in instant failure, the threshold stress ratio (Rc), which is σ_f/σ_s, is expressed by Eq. (6) from Eq. (5) for $\sigma^\infty = \sigma_f$. This equation gives the condition where SOHIC begins to propagate because λ is equal to λ_c under the threshold stress.

$$R_c \equiv \frac{\sigma_f}{\sigma_s} = 1 - \frac{2p\lambda^*}{\sigma_s(1 + \lambda^{*2})^{\frac{1}{2}}},\ \lambda^* \equiv \frac{\lambda}{c} \cdots\cdots\cdots (6)$$

When the hydrogen pressure p is constant, the Rc is determined by the yield strength σ_s around the initiation site and the non-dimensional length λ^* ($= \lambda/c$). In the chain-like SOHIC propagation, the length $2 \cdot c$ is regarded as the length of the initiating crack from a latent initiation site, which is supposedly proportional to the size of the latent initiation site in the stress direction. For instance, the size of a pearlite colony may give the length $2 \cdot c$. Therefore, the fine dispersion of the pearlite colonies makes the length $2 \cdot c$ smaller and the interval λ wider for the larger λ^* values. On the other hand, the banded pearlite colonies show larger $2 \cdot c$ for smaller λ^* because the interval λ is mainly determined by the micro-segregation formed in solidification.

The threshold stress ratio Rc is increased by microstructural controls such as suppressing the formation of banded strucrture by reducing manganese and/or the diffusion treatment, refining the pearlite colonies by the TMCP, and refining the matrix to raise the σ_s. In manufacturing, the TMCP can help prevent SOHIC in terms of the morphological control of the latent initiation sites of the microstructure and the strengthening of the matrix.

Table 1 Chemical compositions of steels tested on HIC- and SOHIC-resistance

Steel	Process	ASTM Grade	Chemical composition (mass%, *ppm)												Ceq (%)	ACR
			C	Si	Mn	P	S*	Cu	Ni	Cr	Mo	V	Nb	Al		
N1	N	A516-70	0.15	0.26	1.15	0.005	7	0.20	0.19	0.01	tr.	0.002	0.018	0.035	0.37	2.45
N2	N	A516-70	0.17	0.25	1.08	0.009	7	0.24	0.24	0.09	0.12	0.029	0.020	0.030	0.43	1.85
TM	TMCP	A841	0.08	0.25	1.15	0.005	7	0.20	0.19	0.01	0.07	0.002	0.023	0.031	0.32	2.38

Notes: "Normalized" is abbreviated for "N". All steels were Ca-treated.

Table 2 Mechanical properties of steels listed in Table 1

Steel	YS (N/mm²)	TS (N/mm²)	El. (%)	YR (%)	50%FATT* (°C)
N1	341	498	26	68	−70
N2	376	547	22	69	−65
TM	505	560	34	90	−79

YS: Yield strength, TS: Tensile strength, YR: Yield to tensile ratio
*By 2 mm-V notch Charpy

4.4 Example of Enhanced SOHIC Resistance by Microstructure Control

The ASTM A516-70 and A841 cl.1 steel plates were investigated for HIC and SOHIC behaviors. Their chemical compositions are listed in **Table 1**. Some characteristics include; the N2 steel contained less manganese than the N1 steel, the TM steel was of low carbon type, and all these steels were of the ultra low S type, and Ca-treated with the ACR values in the optimum range. These plates were rolled to 12.7 mm thickness and finished by two fundamental processes such as the normalizing and the TMCP and denoted as N1, N2 and TM to indicate each process.

Table 2 summarizes the mechanical properties of the steels according to ASTM A20. The N2 steel of the normalized type exhibited higher yield and tensile strength higher than the N1 steel, which was finished by the same process. The actual yield ratio the specified minimum yield strength (SMYS) was 1.31 for the N1 steel and smaller than the N2 steel. On the other hand, the TM steel, A841 cl.1 of the TMCP type, exhibited high yield strength and almost the same ratio to the SMYS as the N2 steel, namely around 1.46. Their microstructures are shown in **Photo 2**. The N1 steel obviously contained pearlite bands. The N2 steel also contained small amount of pearlite, rather dispersed than banded. This difference is attributed to the reduction in the micro-segregation of Mn for the N2 steel with the low Mn content. As for the TM steel, the fine acicular ferrite was dominant with a small amount of polygonal ferrite and finely dispersed quasi-pearlite with deformed carbide lamellas.

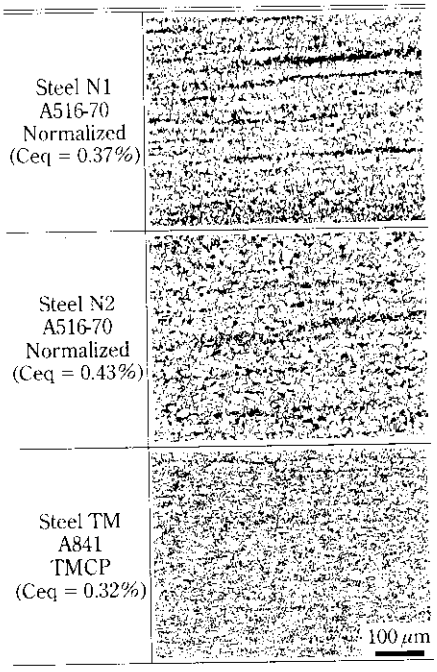

Photo 2 Optical microstructures of steels tested on HIC- and SOHIC-resistance

HIC tests were carries out according to TM0284-96[12] with solution A and the resistance of the steels to SOHIC was evaluated by Method A in TM0177-96[8], *i.e.* constant tensile loading. **Table 3** summarizes HIC and the SSC test results with some measurable latent initiation site model parameters such as σ_s, λ, c and λ^*. The

Table 3 HIC- and SOHIC-resistance of steels listed in Table 1

Steel	HIC Test (CAR %)	Life span in SSC Test		σ_f (N/mm²)	σ_s (N/mm²)	Rc (σ_f/σ_s)	λ (μm)	c (μm)	λ^* (λ/c)
		0.7 SMYS	0.85 SMYS						
N1	0	+	45.2 h	182	341	0.53	22	> 6**	< 3.7
N2	0	+	+	> 221	376	> 0.58	24	6	4
TM	0	+	+	> 302	505	> 0.60	20	< 2	> 10

+: Survived for 720 h, σ_s: Yield strength, σ_f: Failure stress threshold
**Band-like structure

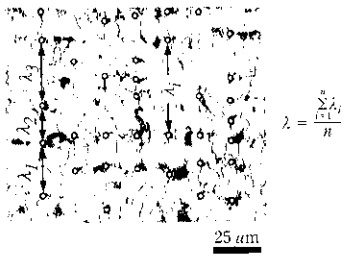

Fig. 8 Measurement of mean interval λ of latent initiation sites

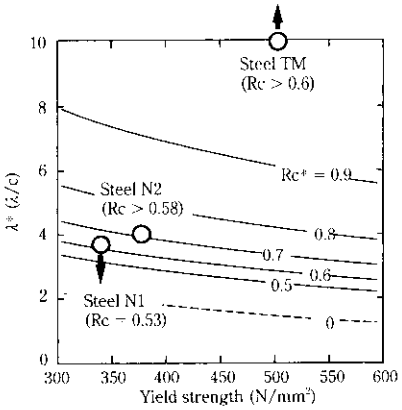

Fig. 9 Effect of microstructure control on SOHIC-resistance of pressure vessel steels. The figures on contours indicate the estimated Rc values, Rc*, by the introduced parameteres based on the latent initiation site model.

values for σ_s should be for the matrix but the yield strength values are given for simplicity. The latent initiation site interval λ is the measurable average of the intervals in the thickness direction by the intersectional method as shown in **Fig 8**. The values of c are averaged equivalent diameters of the second phase such as the pearlite colonies. The largest λ^* value for the N1 steel was estimated to be 3.7 because the c value was presumably the minimum one due to the hand-like morphology of the pearlite. The TM steel had the largest λ^* value of the three, because it had the smallest c value.

The results in Table 3 were plotted over one another in **Fig. 9**, where the estimated contours of Rc (Rc*) were drawn based on Eq. (6). The actual Rc values ($= \sigma_f/\sigma_s$) are shown in the parentheses and the degree of survival is indicated by the signs of inequality. In the case of steels N1 and TM, the λ^* values could not be specified but the known top or bottom values are indicated by the downward or upward arrows, respectively. The accuracy of Rc estimates is not sufficient, but the actual SOHIC resistance evaluated for the three steels agreed with the model estimation.

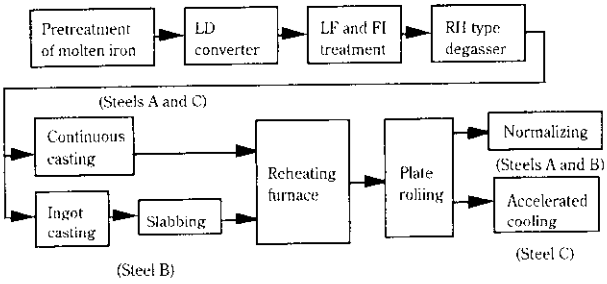

Fig. 10 Manufacturing process of steel plates

5 The Properties of Developed Heavy Gauge HIC Resistant Steels for Pressure Vessels

5.1 Materials

The enlargement of λ^* by the fine dispersion of the latent initiation sites and/or the increase in the yield strength σ_s is quite effective in enhancing SOHIC resistance. The microstructure control by the TMCP is apparently suitable but becomes more difficult as thickness increases. The resistance to HIC and SOHIC and the possible microstructural control were verified from the following two viewpoints for the TMCP application:

(1) In the difficult case where the thickness grows up to 127 mm (88.9 mm for SOHIC evaluation) for the conventional A516–70 steels

(2) In the practical case where the thickness was 50.8 mm for the ASTM A841 cl.1 steel

Table 4 and **Fig. 10** show some specific properties of the plates and the chemical compositions with the manufacturing processes. The A and B steels were of the A516–70 grade and of 88.9 and 127 mm in thickness, respectively. The former was continuously cast steel but the latter was ingot-cast. The steel C was of the A841 cl.1 grade and was continuously cast then subjected to TMCP, which consisted of controlled rolling and accelerated cooling. The C steel was reduced in carbon content to suit the TMCP so that the Pcm value was as small as 0.16 mass%. Improvement in the weldability and low temperature toughness were also apparent. All steels here were minimized in S content with the Ca-treatment for the spheroidization of the sulfide inclusions and also minimized in P content, that is, less than 0.01 mass%, to depress the abnormal structure in the center segregation.

5.2 Tensile Properties of Plates

The tensile properties and the Charpy V-notch impact test results are summarized in **Table 5** with the results of the y-slit cracking test, which was conducted according to JIS Z 3158. The properties after the post-welding heat treatment (PWHT) are also shown. All values in the table satisfy the ASTM specifications. The yield strength was kept rather high and the low temperature toughness was sufficient, as indicated by the energy values at −20°C for steels A and B and at −40°C for steel

Table 4 Chemical compositions of steel plates

(mass%)

Steel	Plate thickness (mm)	Steel grade	C	Si	Mn	P	S	Cu	Ni
A	88.9	A516-70	0.15	0.30	1.14	0.006	0.001	0.19	0.33
B	127	A516-70	0.18	0.30	1.12	0.008	0.001	0.34	0.19
C	50.8	A841cl.1	0.08	0.25	1.15	0.005	0.001	0.20	0.19

Steel	Mo	V	Nb	Ti	Al	Ca	Ceq*1	Pcm*2	ACR*3
A	0.10	0.026	0.018	0.016	0.029	0.003 4	0.40	0.24	2.16
B	0.11	0.024	0.019	0.005	0.035	0.002 0	0.43	0.28	1.58
C	0.07	—	0.023	0.016	0.031	0.002 6	0.31	0.16	2.38

*1 $Ceq = C + Mn/6 + (Cr + Mo + V)/5 + (Cu + Ni)/15$

*2 $Pcm = C + Si/30 + (Mn + Cu + Cr) + Ni/60 + Mo/15 + V/10 + 5B$

*3 $ACR = \{Ca - (0.18 + 130 \cdot Ca) \cdot O\}/(1.25 \cdot S)$

Table 5 Mechanical properties of steel plates

Steel	Plate thick. (mm)	PWHT condition	Location	Tensile test*1			V-Charpy impact test*2			Preheat temp. without cracking*3 (°C)
				YS (N/mm²)	TS (N/mm²)	El. (%)	Absorbed energy (J) −20°C	Absorbed energy (J) −40°C	50% FATT (°C)	
A	88.9	—	1/4 t	380	497	37	195	98	−30	100
			1/2 t	360	506	35	137	59	−16	
		620°C × 7 h	1/4 t	350	486	38	313	77	−29	—
			1/2 t	358	492	35	135	42	−18	
B	127	—	1/4 t	374	523	34	184	91	−32	125
			1/2 t	350	535	32	146	55	−28	
		625°C × 10 h	1/4 t	356	503	35	119	51	−22	—
			1/2 t	362	513	34	93	27	−17	
C	50.8	—	1/4 t	474	573	30	—	452	−75	< 25
			1/2 t	424	547	29		422	−60	
		580°C × 4 h	1/4 t	498	590	30	—	449	−67	—
			1/2 t	454	563	29		439	−48	

*1; T-direction, *2; L-direction, *3; Test procedure; JIS Z 3158

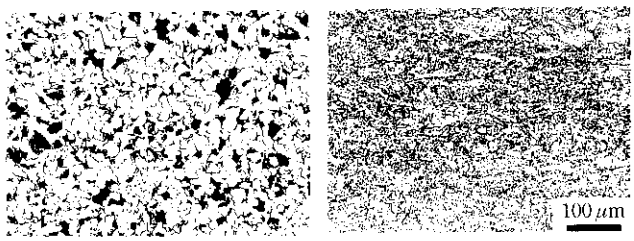

(a) Steel A (A516-70, 88.9 mm^t) (b) Steel C (A841cl.1, 50.8 mm^t)

Photo 3 Optical microstructures of the dreveloped pressure vessel steels

C. The minimum preheating temperature evaluated by the y-slit cracking test was lower than 25°C, which is the value at which preheating may be skipped. **Photo 3** shows the microstructures typical to steels A and C, whose SOHIC resistance was evaluated. A mixture of coarse ferrite and pearlite was found in the normalized steel A. On the other hand, the TMCP steel C shows a fine bainite structure with little pearlite.

5.3 Welded Joint Properties

The performance of the welded joints of three kinds of plates was tested (**Table 6**). The welding method was the submerged arc welding with Kawasaki Steel's consumables (AWS A5.17 F7A6-EH14 equivalent) for the 490 MPa grade steels and its heat input was 27–38 kJ/cm. The mechanical properties of the welded joints after the PWHT are shown in **Table 7**. Each tensile strength value is equivalent to that of each base metal and satisfies the ASTM specification. The toughness in the essential portions such as the weld metal, the fusion line, and the heat-affected zone were evaluated to be high enough for all portions at −20°C for steels A and B, and at −40°C for steel C. The maximum hardness value in the portion 2 mm below the surface was 230 Hv, which is lower than the critical 248.

5.4 HIC and SOHIC Resistance of Base Metals and Welds

The plates and the welded joints mentioned in the previous section were also subjected to an HIC test carried out by the method in NACE TM0284–96[12] with

Table 6 Submerged arc welding conditions

Steel	Plate thickness (mm)	Groove shape (mm)	Number of passes	Current (A) Voltage (V) Velocity (cm/min)	Heat input (kJ/mm)	Preheat and inter-pass temp. (°C)
A	88.9	Doubel V (14°)	BP; 24 FP; 11	480～550 29～34 32～39	31	78～183
B	127	Doubel V (30°)	BP; 50 FP; 14	450～600 29～34 60～62*	38	102～148
C	50.8	X (60°)	BP; 15 EP; 8	480～500 29～31 31～38	27	24～128

Wire × Flux; KW 36 × KB 110 (Corresponding to AWS A5.17 F7A6-EH14), *Tandem electrodes

Table 7 Mechanical properties of SAW joints subjected to PWHT*

Steel	Plate thickness (mm)	Heat input (kJ/mm)	Tensile test	V-Charpy impact test at 1/4 t				Maximum hardness value**
			TS (N/mm^2)	Test temp. (°C)	Absorbed energy (J)			
					WM	FL	HAZ	Hv (98 N)
A	88.9	31	538	−20	340	344	301	230
B	127	38	542***	−20	212	304	333	222
C	50.8	27	560	−40	150	402	447	216

*PWHT condition; 620°C × 7 h (Steel A), 625°C × 10 h (Steel B), 580°C × 4 h (Steel C)
**2 mm below the surface
***Average of results of two test specimens taken from the top and the bottom portions

Table 8 HIC test results of steel plates and welded joints

Steel	Plate thickness (mm)	PWHT condition	Thickness-wise position	Cracking ratios (%)					
				Base plate			Welded joint		
				CLR	CTR	CSR	CLR	CTR	CSR
A	88.9	—	Surface	0	0	0	0	0	0
			1/2 t	0	0	0	0	0	0
		620°C × 7 h	Surface	0	0	0	0	0	0
			1/2 t	0	0		0.2	0	0
B	127	—	Surface	0	0	0	0	0	0
			1/2 t	0.3	0	0	0.2	0	0
		625°C × 10 h	Surface	0	0	0	0	0	0
			1/2 t	0.1	0	0	0.2	0	0
C	50.8	—	Surface	0	0	0	0	0	0
			1/2 t	0	0	0	0.2	0	0
		580°C × 4 h	Surface	0	0	0	0.1	0	0
			1/2 t	0	0	0	0	0	0

*Test procedure; NACE TM0284-96, Test solution; A, Test specimen; 30 mm thick

solution A. The results are summarized in **Table 8**. They were quite satisfactory, with a small error of 0.3% CLR-value at maximum.

The SSC test was carried out by method A (tensile type) in NACE TM0177–96 with solution A on steels A and C. The test results are summarized in **Table 9**. The threshold stress ratio was estimated to be 60% for the A steel of the A516-70 grade with coarse microstructure. This percentage was slightly smaller than the N1 steel mentioned in Chapter 4 and was associated with the decrease in the λ^* value due to the coarsening of the microstructure. PWHT made the results worse. The decrease in the yield strength may have been a cause of this phenomena. On the other hand, steel C, with its very fine bainite structure, exhibited such remarkably good SOHIC resistance that the threshold stress ratio was 90% for the A841 cl.1 grade, being free of the detrimental influence of the PWHT.

Table 9 SSC test* results of steel plats and welded joints

Steel	Plate thickness (mm)	PWHT condition	Thickness-wise position	Life span for load ratios to SMYS (h)					
				Base plate			Welded joint		
				0.6	0.7	0.9	0.6	0.7	0.9
A	88.9	—	1/4 t	+	115	–	+	+	40
			1/2 t	+	+	–	+	+	+
		620°C × 7 h	1/4 t	+	294	–	+	34	52
			1/2 t	+	252	–	+	64	23
C	50.8	—	1/4 t	–	+	+	–	+	+
			1/2 t	–	+	+	–	+	+
		580°C × 4 h	1/4 t	–	+	+	–	+	+
			1/2 t	–	+	+	–	+	+

*Test procedure; NACE TM0177-96, Method A, Test solution; A, Test period; 720 h
**SMYS; 260 N/mm^2 for steels A and B, 345 N/mm^2 for steel C
+: Survived for 720 h
–: No test

6 Conclusion

The current status of technologies to suppress the HIC susceptibility of various steel grades was reviewed and SOHIC mechanism was examined in order to find out the essential factors for manufacturing heavy-gauge pressure vessel steel plates with advanced HIC and SOHIC resistance. The conclusions are summarized as follows:

(1) The current shape control of MnS has been successfully established for the high HIC resistance. It controls the ACR values within the optimum range, namely from 1 to 3, by the Ca-treatment together with lowering S and O content.

(2) The characteristic cracking behavior of SOHIC has been clarified by the latent initiation site model in which the initiation sites are activated by the interaction between the applied stress and hydrogen pressure.

(3) The latent initiation site model gave the following microstructural control guidelines to enhance SOHIC resistance: (a) the rise of the matrix yield strength, and (b) enlargement of the interval between the latent initiation sites by the fine dispersion of the pearlite colonies for instance, TMCP is most suitable for these controls.

(4) The TMCP steel of the A841 cl.1 grade for pressure vessel use exhibited the best SOHIC resistance owing to its fine microstructure.

(5) The developed pressure vessel steels of 88.9 and 127 mm in thickness for the A516–70 grade and of 50.8 mm in thickness for the A841 cl.1 grade were manufactured and judged to be satisfactorily resistant to HIC. The A841 steel exhibited especially high SOHIC resistance, as well as good HIC resistance.

(6) All the developed steels were also verified to have good weldability and joint performance as well as the low hardness, which are desirable qualities for SSC resistance.

References

1) Y. Kobayashi, K. Ume, T. Hyodo, and T. Taira: *Corrosion Science*, **27**(1987)10, 1117–1135
2) C. Fowler and F. Golightly: Pipeline Tech. Conf. Part B, (1990), 18.33–18.46
3) T. Kaneko, M. Takeyama, M. Nakanishi, Y. Sumitomo, and A. Ikeda: Proc. Middle East NACE Corrosion Conf., Bahrain, (1979)
4) H. Takehiro, T. Yoshino, N. Yurioka, and M. Abe: Proc. of the 8th Int. Conf. on Offshore Mechanics and Arctic Engineering at the Hague, V(1989), 339–346
5) O. Haida, T. Emi, K. Sanbongi, T. Shiraishi, and A. Fujiwara: *Tetsu-to-Hagané*, **10**(1978), 1538–1547
6) O. Haida, T. Emi, G. Kawanishi, M. Naito, and S. Moriwaki: *Tetsu-to-Hagané*, **12**(1980), 354
7) M. Kimura, N. Totsuka, T. Kurisu, K. Amano, J. Matsuyama, and Y. Nakai: Corrosion 1986, March, Houston (Texas), paper 160
8) NACE Standard TM0177–96: "Standard Test Method Laboratory Testing of Metals for Resistance to Specific Forms of Emvironmental Cracking in H2S Environments"
9) K. Amano, F. Kawabata, J. Kudo, T. Hatomura, and Y. Kawauchi: "High Strength Steel Line Pipe with Improved Resistance to Sulfide Stress Corrosion Cracking for Offshore Use", Proc. of the 9th Int. Conf. on Offshore Mechanics and Arctic Engineering, V(1990), 21–26
10) M. Iino: *Tetsu-to-Hagané*, **64**(1978)10, 1578
11) F. de Kazinczy: *Acta Met.*, **7**(1959), 525
12) NACE Standard TM0284–96: "Standard Test Method Evaluation of Pipeline Pressure Vessel Steels for Resistance to Hydrogen Induced Cracking"